CORE
Metadata, citation and similar papers at core.ac.uk
Provided by Digital.CSIC

Structural and electrical properties of indium oxide thin films grown by Pulsed Laser Deposition in oxygen ambient

Jolanta Stankiewicz[a], Xavier Torrelles[b], José Luis García-Muñoz[b], Javier Blasco[a]

[a] *Instituto de Ciencia de Materiales de Aragón and Departamento de Física de la Materia Condensada, CSIC–Universidad de Zaragoza, 50009-Zaragoza, Spain*
[b] *Institut de Ciència de Materials de Barcelona, ICMAB-CSIC, E-08193 Bellaterra, Spain*

Abstract

We report results of structural, optical and electrical transport studies of indium oxide (IO) thin films grown by Pulsed Laser Deposition (PLD) under various oxygen gas pressures and using different substrates at 350 °C. We find that the morphology and electrical resistivity of these films which are highly transparent changes drastically as O_2 pressure increases into mbar range, irrespective of substrate. A systematic increase in resistivity, coming mainly from a drop in the electron concentration, is observed as oxygen pressure varies from 0.0004 to 1 mbar. This could permit modulation of IO thin–films' electrical parameters by more than three orders of magnitude suggesting that PLD grown films could be an attractive material for optoelectronic applications.

Keywords: indium oxide thin films electrical properties

1. Introduction

Transparent conducting oxide (TCO) films are used in multiple applications, from touch panels and flat panel displays to low emissivity windows, and gas sensors [1, 2, 3, 4, 5]. Indium oxide (IO) is one of the most widely applied TCO materials, not only as a conducting electrode but also as an active component of devices [6, 7]. Its research has been centered almost entirely on heavily doped *n*-type films in search of highly transparent material with nearly metallic conductivity. In particular, indium oxide doped with tin (ITO) is probably the most studied TCO. The tin doping increases the carrier concentration, most likely by substituting for indium and acting as a singly charged donor on an indium site. In spite of many reports, some fundamental properties of IO are only just coming out. Thus, an important improvement in material quality has enabled to establish the nature of the IO band gap [8]. Nevertheless, the

Email address: jolanta@unizar.es (Jolanta Stankiewicz)

origin of a high free–electron concentration in as-grown thin films remains under dispute. In part, it follows from the fact that existing models for In_2O_3 doping are inconclusive [9, 10, 11, 12], although it is clear that native defects are relevant as dopants in this transparent oxide. In addition, systematic studies focused on tailoring of the indium oxide electrical properties in a broad range are missing although such research would open the way to new applications in thin film opto–electronics, particularly in photovoltaics [13, 14, 15, 16].

Indium oxide crystallizes in a cubic bixbyite structure, which derives from the fluorite structure when one fourth of the oxygen atoms is removed. The structural vacancies in the bixbyite structure are actually empty interstitial positions which can serve as fast oxygen diffusion paths and thus favor easy incorporation of oxygen ions into the material [17]. As–grown IO samples show rather high conductivities, most likely brought about by presence of oxygen vacancies which act as a shallow donor. This has been corroborated by first–principles calculations [11, 18] and annealing experiments [19]. It is now generally accepted that oxygen doping plays the fundamental role for indium oxide physical properties [20, 21]. In the thin–film form, the unique crystal-defect structure of bixbyite based materials prompts segregation of oxygen at the grain boundaries (GB). This can give rise to charged interface states and, consequently, to GB potential barriers. Such barriers can affect, to a large extent, electronic transport of polycrystalline thin films [22], in particular of indium oxide [23]. On the other hand, the surface accumulation layer seems to contribute insignificantly to the IO–film conductivity [24].

The great majority of the published papers on TCO is limited to description of fabrication methods and improvement of ensuing film properties. Surprisingly, only few reports deal with physical mechanisms behind the measured properties at the fundamental level. In this report, we show how the oxygen ambient affects the microstructure and electrical behavior of IO thin films grown by pulsed laser deposition (PLD). We choose to study indium oxide and not ITO in order to avoid ambiguities related to the tin doping which gives rise to several defect complexes [25]. To elucidate the physical mechanism behind found behavior, we have performed a careful structural characterization of the films, in addition to electrical and optical measurements. We find that films morphology and its electrical properties, which vary in a systematic way with O_2 background pressure applied during PLD growth, are closely correlated. The background oxygen promotes stoichiometric film formation as oxide deposition. It also leads to the conductivity decrease since the number of donor oxygen vacancies in films becomes smaller upon O_2 doping during growth. Even though at lower pressures the presence of oxygen favors a highly textured columnar growth with smooth surface, at elevated pressures it gives rise to more defective structures with more localized electronic transport. The observed behavior can be attributed to variations in the plume of ejected material and in surface diffusion brought about by changes in oxygen pressure in the PLD process [33].

The PLD deposition method has successfully been used to obtain IO [26, 27, 28, 29] and indium–tin–oxide thin films [30, 31]. It yields high-quality films of a variety of materials and is simple in operation as only a few parameters such as

the laser energy density, the pulse repetition rate, the substrate temperature, and the deposition pressure need to be controlled. Although usually obtained as a highly conducting *n*-type material, our IO thin films grown by PLD under various O_2 pressures, up to 1 mbar, show systematic increase in resistivity which spans more than two (four) orders of magnitude at 300 K (4 K). The resistivity increase is coming mainly from the electron concentration decrease; however, the carrier mobility variation for O_2 pressures beyond 0.1 mbar is also important. This finding offers a new opportunity to tune IO films properties by choosing proper growth parameters. The optical transparency of all films is high ($\gtrsim 80\%$) in the spectral range from 400 to 800 nm.

2. Experiment

We have grown IO thin films by pulsed laser deposition from a ceramic IO commercial target in a vacuum system with a base pressure better than of $\sim 1 \times 10^{-6}$ Torr. Fused-quartz, GaAs(100), and Si(100)-oriented wafers have been used as substrates which were kept at a constant temperature between 350 ° and 500 °C. The O_2 gas pressure during deposition was fixed at various values between 0.0004 and 1 mbar. A total of 2500 pulses with repetition rate of 10 Hz was applied, using a KrF excimer laser at energies of 65 mJ and a fluence of 1.8 J/cm^2. After deposition, the films were cooled down to room temperature (RT) at the oxygen pressure used for the growth. The cooling rate of 20 °C/min was employed down to 250 °C, followed by free cooling to RT. For the x–ray diffraction (XRD) characterization, a Siemens D-5000 (λ[Cu K_α]= 1.541840 Å) and a Bruker-AXS D8 Advance diffractometer with general area detector diffraction system (GADDS) were used. The crystallinity of IO films was evaluated from the full–width at half maximum (FWHM) of the (222) diffraction peak in XRD spectra. Field emission scanning electron microscope (FESEM), in both plane and cross-section views, was used to study films' morphology. We applied low voltage to get our FESEM images in order to ensure more sensitivity to surface features and to be able to observe directly nonconducting samples. The Van der Pauw method was used to obtain the resistivity and Hall effect data in magnetic fields of up to 1 T. Experimental errors coming from geometrical effects were minimized by placing contacts on the corners of a $\sim$ 3 mm x 3 mm squares cut from the films. At least two samples, cut from the same batch, were measured in order to check for homogeneity. We used an electrometer with a guarding option to perform measurements on high resistance films. Ohmic contacts to the layers were done using Au or silver paste. Optical transmission spectra of the films were measured by a dual-beam Cary spectrophotometer.

3. Results and Discussion

3.1. Structural and morphological properties

All the layers deposited by PLD on Si(100) and GaAs(100) substrates were found to crystallize in the pure bixbyite structure. In these films only peaks

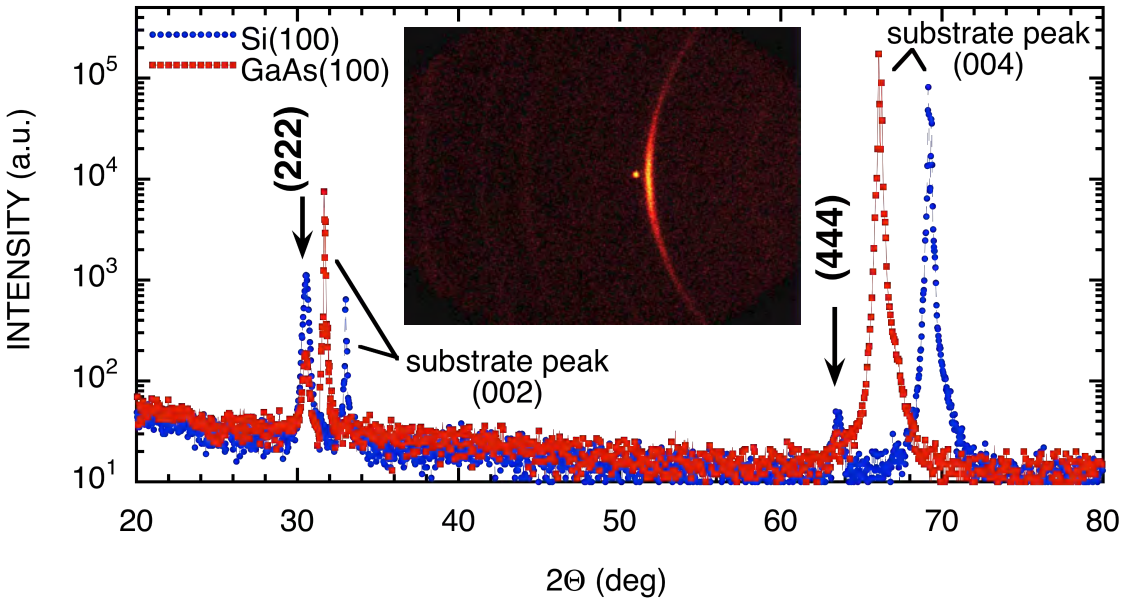

Figure 1: (Color online) Full XRD scans for films deposited at p_{O_2} = 0.1 mbar on Si(100) and GaAs(100) substrates. The inset shows two-dimensional GADDS image for a In_2O_3 film grown on GaAs(100). The dot and the ring correspond to the (002) substrate and (222) cubic reflections of the film, respectively. The distribution of intensity indicates a texture perpendicular to the surface.

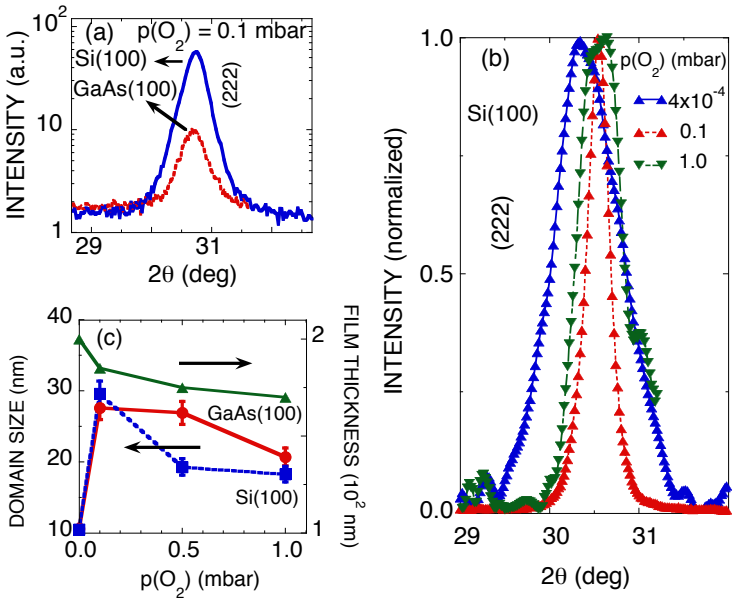

Figure 2: (Color online) (a) (222) diffraction peak for films deposited at p_{O_2}= 0.1 mbar on Si(100) and GaAs(100) substrates; (b) normalized and smoothed (for a better visualization) X-ray diffraction spectra at their corresponding peak maximum for In_2O_3 films grown by PLD at various O_2 pressures on Si(100) substrate; (c) pressure variation of mean crystalline domain size (left axis) and of film thickness (right axis).

corresponding to (222) and (444) planes are clearly distinguished in the XRD patterns indicating preferential (111) texture. This is seen in Fig. 1 which shows full scans for films grown at p_{O_2}= 0.1 mbar on Si(100) and GaAs(100) substrates. For the latter, the (444) peak is hardly discerned but it can be unambiguously identified. The texture found is expected for the In_2O_3 bixbyite phase, since it corresponds to the lowest surface free energy. The (222) and (444) peaks, approximately at 31° and 64°, appear very close to the peaks from the crystalline substrates. The observed growth is columnar, of Volmer–Weber type (not epitaxial), with a high degree of texture which depends on oxygen pressure but with a poor in-plane (lateral) order between columns, even in the best films. The films preferentially grow along the diagonal cubic lattice direction, perpendicular to the substrate surface. The inset of Fig. 1 shows the GADDS image for the film on GaAs(100) substrate. The image is centered on the (002) substrate peak and exhibits a ring with the maximum intensity at the (222) IO film reflection. This corroborates the vertical (111) texture, in agreement with the fact that the (222) plane has the lowest surface energy. On the other hand, the 2D diffraction patterns (GADDS), obtained at different azimuthal angles up to 100° for the films, show no intensity variations (see Fig. S1 of the Supplementary Material). Therefore, the degree of texture is much lower in the surface plane, indicating lack of lateral order. We found no substantial variation between films grown at temperatures between 350 ° and 500 °C (see Fig. 1 and Fig. S2 of the Supplementary Material). In what follows, we present the results for films grown at the substrate temperature of 350 °C with the aim to compare them to those obtained for films deposited by dc magnetron sputtering that we had studied earlier [21, 23].

Figure 2(a) shows the main (222) peak in the XRD spectra obtained for the films grown on Si(100) and GaAs(100) substrates at p_{O_2}=0.1 mbar. Higher intensities were systematically recorded for Si(100) although similar peak widths are found in both cases. On the other hand, clear variations in the peak width are observed varying the O_2 pressure. This is illustrated in Fig. 2(b) which shows the normalized (222) peak width for various values of p_{O_2}. The perpendicular crystallite size in the layers was estimated from the FWHM of the (222) diffraction peaks, such as shown in Fig. 2(b), applying the Debye–Scherrer formulae. The values thus obtained (after deconvolution of the instrumental resolution) are plotted as a function of oxygen pressure in the Fig. 2(c). Overall, the mean sizes of crystallites do not depend on the nature of the substrate as they are nearly the same for Si(100) and GaAs(100). They do mainly depend on the O_2 pressure applied during growth: the increase in p_{O_2} up to 0.1 mbar gives rise to larger crystallites. Beyond this pressure value the size of the coherent crystalline domains systematically decreases. A slight variation in the peak position, observed at very low O_2 pressures (see Fig. 2(b)), can be attributed to changes in the oxygen content and to possible relaxation effects associated to texture. The peak at (222) reflection, for the film deposited on Si(100) substrate at p_{O_2}= 0.5 mbar, is barely seen. This particular layer, as shown below, is less dense and more disordered than the others. Hereafter (in absence of any other specification), by "domain size" or "crystallite size" in the text we mean the

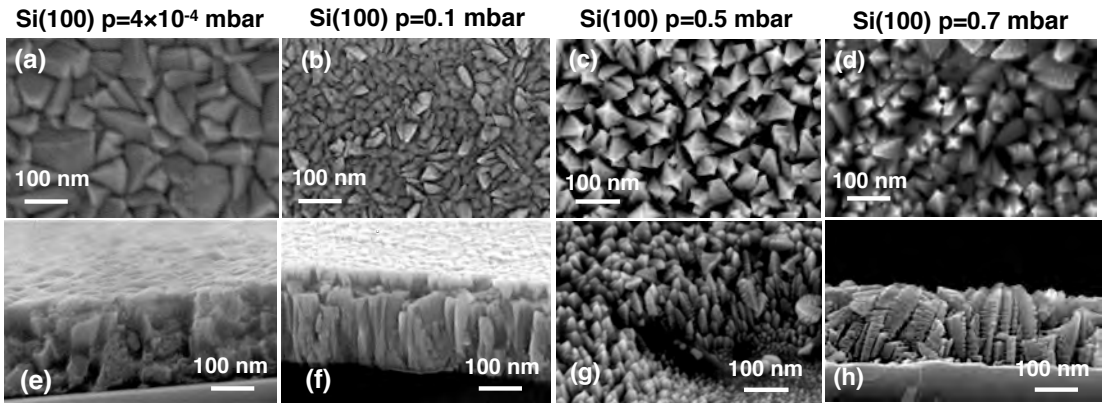

Figure 3: Surface and cross-sectional FESEM images of In_2O_3 grown by PLD at 350 °C on Si(100) substrate at various O_2 pressures: (a),(e) 4×10^{-4} mbar; (b),(f) 0.1 mbar; (c),(g) 0.5 mbar, and (d),(h) 0.7 mbar.

size perpendicular to the surface.

Figure 3 shows how the films' morphology and texture varies with oxygen pressure in FESEM plane and cross–sectional views. No significant differences are seen in the film growth between Si(100) and GaAs(100) substrates. Therefore, we show representative images only from the Si(100) deposition. The grain boundaries in the films are easily distinguished from the surface morphology. However, intra–granular fractures during cleavage cause the boundaries less visible in cross–sectional views. The border between the substrate and the IO film, although not exactly flat, is abrupt for all films studied. At the lowest O_2 pressure ($p_{O_2} = 4\times10^{-4}$ mbar), the (222) peak is broader and its intensity is of about 25 times weaker than that in the best film. Even though the crystalline grains seem to have dimensions close to 60 nm, as estimated from the top SEM view (Fig. 3(a)), the coherence of the crystalline domains perpendicular to the surface is around 10 nm (Fig. 2c). In addition, the typical columnar growth is hardly appreciable in Figs. 3(a,e). The films' quality becomes better as the O_2 pressure gets higher. The films grown at $p_{O_2} = 0.1$ mbar exhibit much smaller FWHMs of (222) peaks than the other layers. The corresponding growth is columnar through the films thickness ($\approx$ 200 nm) although some discontinuities along columns direction can be observed (see Fig. 3(f)). The perpendicular dimension of the crystals, estimated from the XRD spectra, is about 30 nm, quite close to the columns width seen in the SEM images. Moreover, several regions with identically oriented crystals can be distinguished in the plane view of these films (Fig. 3(b)). Similar growth morphology is observed for films obtained at 475 °C (Fig. S3 of Supplementary Material).

At oxygen pressures beyond 0.1 mbar, the films' growth remains highly textured although some distinct trends emerge in FESEM images (see Fig. 3). The films are more polycrystalline, with less dense structures, and more rough

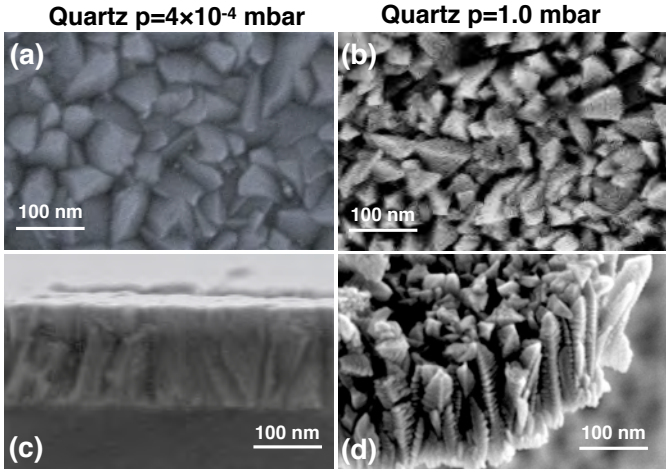

Figure 4: Surface and cross-sectional FESEM images of In_2O_3 grown by PLD at 350 °C on fused quartz substrate at (a),(c) 4×10^{-4} mbar and (b),(d) 1.0 mbar O_2 pressure. The image (d) corresponds to cross-sectional view of a free–standing piece of the film.

surfaces than the layers deposited at lower oxygen pressures. The increased surface roughness comes in part from prismatic faceting which appears at these pressures. The perpendicular grain size decreases from approximately 30 nm to 20 nm as the O_2 pressure increases to 1 mbar. Interestingly, the columnar grains exhibit lateral nano–dendrites, perpendicular to the growth direction. No such features have been observed in the sputter–grown IO films. Most likely, this comes from the effects of the background oxygen pressure on the ablation process through the plume slowing and/or its thermalization [33]. The misorientation of grains is larger for the IO layers grown on amorphous quartz (see Fig. 4 and Supplementary Material) than for the films deposited on Si(100) or GaAs(100).

The morphological evolution of the IO thin films studied can tentatively be explained by variations in the plume features and in surface diffusion arising from changes in oxygen pressure. First, we note that the films structural properties show very weak dependence on the nature of the substrate as they are nearly the same for Si(100) and GaAs(100). This points to the presence of native oxides on both substrates. Therefore, the first few atomic layers of the IO films would be almost randomly oriented as they do not nucleate epitaxially anchored to the surface. The preferred (111) orientation, which minimizes the surface energy, is gained later in the growth when the film thickness develops [34, 35]. The IO films deposited at very low O_2 pressures are quite disordered and show some intercolumnar porosity. It may be attributed to the plume splitting into a fast (collision–less) and a slow (scattered) component in the deposition process and/or to low atomic mobility. As the pressure of the background oxygen gets higher, it promotes stoichiometric film formation as oxide deposition. With a PLD target-substrate distance around a few centimeters, the plume particles

can thermalize completely at $p_{O_2} \gtrsim 0.1$ mbar. In addition, the deposition rate increases leading to larger adatom energies. Since the surface diffusion is significant at the substrate temperature of 350 °, the IO films grow as crystalline columns with less defects and larger grain size. Further increase in the O_2 pressure, however, decreases the energy of particles reaching the substrate due to collisions of the ablated particles with gas molecules. Consequently, the particle migration on substrate surface diminishes and ensuing columnar growth becomes less crystalline with smaller grain size, which may be facetted at the surface. The elevated oxygen pressure can also constrain the expansion of the plume of ejected material in the PLD process and enhance probability of material re-deposition onto the target surface [33].

Summarizing, we find that the morphology of the IO films grown by PLD depends strongly on the oxygen pressure but not on the nature of substrate and only slightly on its temperature in the range studied. Both FESEM and XRD studies show a high degree of (111)-textured columnar growth for IO layers deposited at oxygen pressure close to 0.1 mbar on Si(100) and GaAs(100) substrates. However, these films demonstrate a large lateral disorder with various in–plane orientations.

3.2. Electrical transport and optical properties

Let us now discuss electrical transport in the PLD grown thin films. Figure 5 shows how the resistivity ρ of the thin films grown in O_2 environment varies with temperature. All films, except the ones obtained at the lowest O_2 pressure, show semiconducting behavior. Remarkably, the rise in the O_2 pressure from about 0 to 1.0 mbar leads to more than three orders of magnitude increase in the resistivity of the films. This increase is mainly brought about by a decrease in carrier concentration as ambient oxygen pressure during PLD growth gets higher. This is shown in the upper panel of Fig. 6. Nevertheless, carrier mobility decrease for $p_{O_2} \gtrsim 0.1$ mbar is also important (see the lower panel of Fig. 6). Interestingly, in the range studied, the room–temperature carrier concentration n(300K) varies nearly as inverse of the square root of oxygen pressure ($n \propto 1/\sqrt{p_{O_2}}$). It is not so for 5 K where n starts to drop more rapidly at $p_{O_2} \gtrsim 0.2$ mbar.

The PLD films are of n-type at 300 K as confirmed by the sign of the Seebeck and Hall effects. The room-temperature carrier mobility (~ 25 cm^2/Vs) of the films grown at low oxygen pressure compares favorably with MBE-grown single-crystalline IO films [36]. Larger values of p_{O_2} during growth lead to smaller values of carrier mobility although not so low as for the films grown by sputtering at 350 °C and 1 mbar of O_2 (which are below 1 cm^2/Vs at 300K). However, the sputter–grown films in oxygen ambient exhibit p-type conductivity [21]. Positive sign of the Hall effect at low temperatures is found as well for the film deposited at 0.5 mbar on Si(100). As can be seen from the XRD patterns and FESEM images (Fig. 3), the structure of this film is less dense and more disordered than that of other films. Its surface is quite irregular and electrical resistivity abnormally high as compared to the rest of the IO layers. For these reasons, we do not include results obtained for this particular film in our discussion.

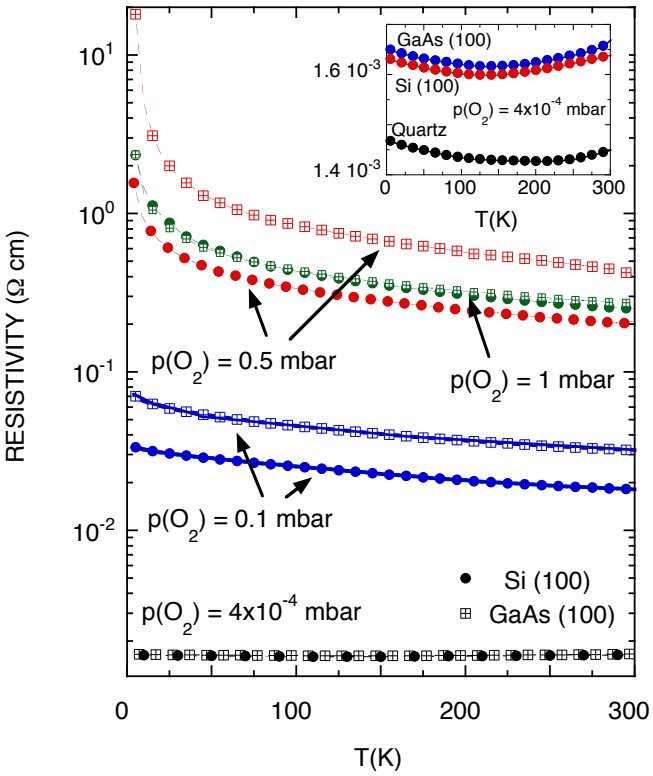

Figure 5: (Color online) Electrical resistivity variation with temperature for IO films grown by PLD at various ambient oxygen pressures. The solid lines for p_{O_2}=0.1 mbar are the fits of the fluctuation-induced-tunnelling model to experimental data. The inset shows $\rho(T)$ at p_{O_2}=4×10^{-4} mbar on linear scale.

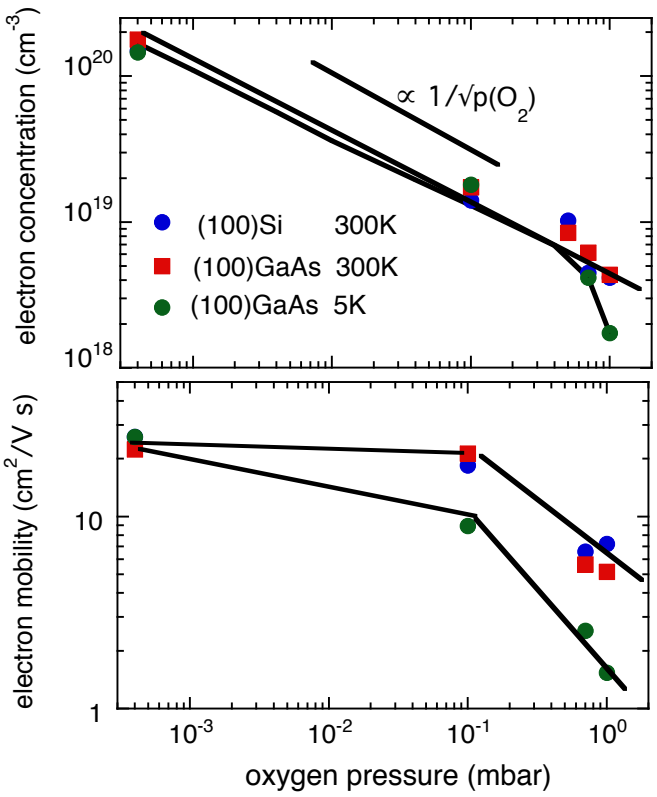

Figure 6: (Color online) Electron concentration (upper panel) and electron mobility variation with oxygen pressure for IO films grown by PLD at 350 °C. The solid lines are guides to the eye.

Table 1: Transport and variable–range hopping parameters obtained for In_2O_3 films from resistivity measurements.

	In_2O_3 on (100)Si				In_2O_3 on (100)GaAs			
$p(O_2)$ mbar	ρ(300 K) Ω cm	ρ(4 K) Ω cm	T_0 K	$N(E_F)$ $eV^{-1}cm^{-3}$	ρ(300 K) Ω cm	ρ(4 K) Ω cm	T_0 K	$N(E_F)$ $eV^{-1}cm^{-3}$
0.5	0.425	35	—	—	0.204	1.89	4650	$1.1{\cdot}10^{22}$
0.7	0.249	1.82	3340	$1.6{\cdot}10^{22}$	0.188	1.55	4750	$1.07{\cdot}10^{22}$
1.0	0.275	3.12	5500	$9.2{\cdot}10^{21}$	0.253	3.17	6000	$8.6{\cdot}10^{21}$

The IO films grown by PLD in O_2 ambient are disordered systems near to the Anderson–localization regime in their electrical transport properties. None of grain–barrier contributions to electrical transport is found in the films. This is to be expected since the electron mean free path $\lambda = (\hbar/e)k_F\mu$, which in our films is below 30 Å, is much smaller than the crystalline grain size. Here, $k_F = (3\pi^2 n)^{1/3}$ is the Fermi wave number and μ is the electron mobility. The films grown at $p \approx 0$ show almost metallic behavior of degenerated semiconductor (see inset of Fig. 5). In these films, the electron concentration is above the critical Mott concentration of metal-insulator transition ($n_{Mott} \approx 5.5 \times 10^{18}$ cm^{-3} for In_2O_3) [37, 39]. In the IO films grown at higher O_2 pressures, current carriers become localized. The transport models for systems in this regime involve mainly phonon-assisted hopping or tunnelling. As shown below, the variable-range hopping (VRH) model fits $\rho(T)$ data best for our films grown at $p_{O_2} \geq 0.5$ mbar. However, none of the hopping versions fits the data for the films deposited at intermediate p_{O_2} pressure (0.1 mbar). We find that the fluctuation-induced-tunnelling (FIT) model which has been applied to several disordered metallic systems and metal-insulator composites [41] is appropriate to calculate the conductivity for this case.

Figure 7 show how $\log(\rho(T)/T^{1/2})$ varies with $1/T^{1/4}$ for the films grown on (100)Si and (100)GaAs substrates at $p_{O_2} \geq 0.5$ mbar. The experimental data points for these films fall on straight lines for $T \lesssim 120$ K. Therefore, the resistivity of these films follows the variable-range hopping (VRH) behavior: $\rho(T)/T^{1/2} = \rho_0\ exp[(T_0/T)^{1/4}]$ [37] at low temperatures. The parameter T_0 of the VRH model is given by: $T_0 = 18/k_B a^3 N(E_F)$ [38], where k_B is Boltzmann constant, a is the localization length, and $N(E_F)$ is the density of states at the Fermi level, respectively. Fitting the above relation to the experimental resistivity results, we obtain T_0 values shown in Table I. It is then possible to calculate $N(E_F)$. To this end, we assume that the electronic localization length is equal to the effective Bohr radius of the shallow donors. For In_2O_3, its value is of 1.6 nm for the major shallow donors, such as oxygen vacancies or hydrogen impurity atoms [39]. The estimated in this way values of $N(E_F)$ (see Table I) are comparable to other oxide films [40]. Solid lines in the inset of Fig. 7 display the fit of the VRH model to the experimental data for two films grown on (100)GaAs substrate.

The resistivity of the PLD films grown at $p_{O_2} = 0.1$ mbar does not follow the

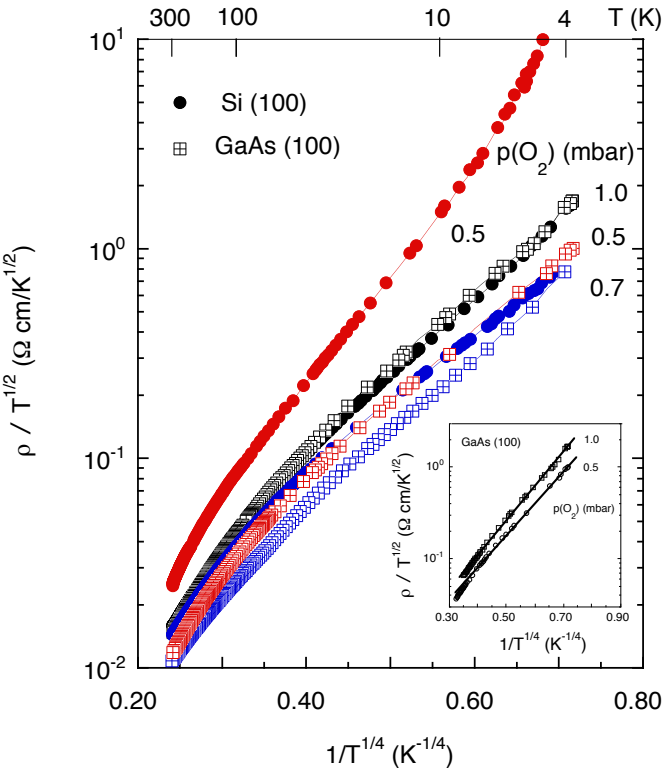

Figure 7: (Color online) Electrical resistivity variation with inverse of $T^{1/4}$ for IO films grown by PLD at various oxygen pressures. The inset shows the fits of the VRH model (solid lines) to experimental data for two films grown on (100)GaAs.

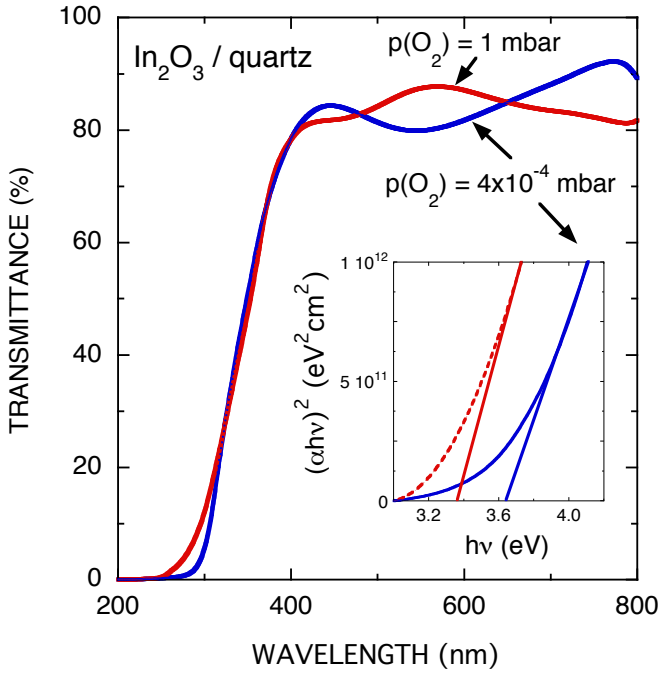

Figure 8: (Color online) Transmittance spectra of IO films grown by PLD on amorphous quartz at p_{O_2}=4×10^{-4} and 1 mbar. Inset shows plot of $(\alpha h\nu)^2$ versus $h\nu$ in the fundamental absorption region.

hopping models nor grain boundary scattering predictions. The solid lines in Fig. 5 are calculated according to the FIT model [41], for which $\rho \propto exp[T_1/(T+T_0)]$. In this model, the charge transport is limited by tunnelling across thin insulating barriers which separate large conducting regions. The tunnelling probability, and hence also the conductivity, depends on the fluctuation of the thermal voltage across the barriers. The parameters T_1 and T_0 are related to the properties of the insulating barriers between the conducting regions. We find $T_1 \approx 170$ K (380 K) and $T_0 \approx 150$ K (310 K) for the layers grown on (100)Si ((100)GaAs), which is close to the values found for tin-doped indium oxide nanoparticles systems [42].

In general, it is clear from our transport data that the oxygen ambient in the PLD growth affects importantly electrical properties of IO films leading to more resistive layers as the O_2 pressure gets higher. The conductivity decrease is readily understandable since the number of donor oxygen vacancies in films becomes smaller upon O_2 doping during growth. The presence of oxygen gives also rise to more defective structures most likely through constraining the expansion of the plume of ejected material in the PLD process and an enhanced probability of material re-deposition onto the target surface [33]. In addition, collisions of the ablated particles with gas molecules lead to lower surface diffu-

sion since the energy of particles reaching the substrate decreases. This affects not only morphology of the films but also their electrical transport as the current carriers become more localized. These two properties are correlated and can be tailored by choosing proper growth's parameters.

Finally, we comment on optical properties of indium oxide films obtained in this investigation. Figure 8 shows how the transmittance of the films grown on amorphous quartz varies with wavelength in the range from 200 to 800 nm. Interference effects modulate somewhat the optical response but all films show transparency beyond 80% in the visible range. Their transmittance is comparable to that of *n*–type IO films [1]. The fundamental absorption starts from about 380 nm. The absorption coefficient α reaches values exceeding 10^5 cm^{-1} at the higher photon energies, as expected for direct-allowed transitions [43]. We obtain α using the relation $T = exp(-\alpha d)$, where T is the transmittance and d is the film thickness. Thus, the optical band–gap can be estimated by extrapolating to zero absorption the linear part of the plot which relates the absorption coefficient and the incident photon energy $h\nu$: $(\alpha h\nu)^2 = A(h\nu - E_g)$ [44]. Here, A and E_g are optical constant and optical band–gap, respectively. The inset of Fig. 8 shows such plots for two films grown on amorphous quartz. We observed that the band–gap decreases going from an almost metallic film deposited at p_{O_2}=4×10^{-4} mbar to a highly insulating one grown at p_{O_2}= 1 mbar, in agreement with Burstein-Moss shift which widens the optical energy gap upon increasing doping [45].

3.3. Concluding remarks

In summary, crystalline indium oxide films with the cubic bixbyite structure were obtained by PLD method at 350 °C in varying oxygen ambient. In addition to their high transparency in the visible spectral range, the electrical properties of the films can be tailored as a function of background gas pressure. The rise in the O_2 pressure from about 0 to 1.0 mbar leads to increase in the resistivity of the films by more than three orders of magnitude. This variation comes mostly from a decrease in carrier concentration. The experimental data show that the more resistive films are disordered semiconducting systems close to the Anderson–localization regime. Their conductivity can be modeled by the variable–range hopping and fluctuation-induced-tunnelling models. The films' morphology variation with O_2 background pressure follows that of electrical transport properties disclosing correlation between them. More conducting films show denser columnar microstructure with fewer defects and smoother surfaces.

These findings reveal the importance of oxygen background gas for properties of indium oxide thin films grown by PLD. They also open way to the optimization of the growth conditions in order to obtain transparent material with desired carrier concentration for multiple uses as transparent conducting electrodes or substrates in photovoltaic cells.

4. Acknowledgement

We acknowledge support from grants MAT2012-38213-C02-01 and -02, and MAT2015 -686760-02-1-P and -2-P from the Ministerio de Economía y Competividad of Spain. These grants are co–funded by ERDF of European Union. Additional support from Diputación General de Aragón (DGA-CAMRADS) is also acknowledged. We used Servicio General de Apoyo a la Investigación-SAI of Universidad de Zaragoza in our research.

References

[1] I. Hamberg, C.G. Granqvist, J. Appl. Phys. 60 (1986) R123.

[2] B.G. Lewis, D.C. Paine, MRS Bulletin 25 (2000) 22.

[3] C.G. Granqvist, A. Hultåker, Thin Solid Films 411 (2001) 1.

[4] E. Fortunato, D. Ginley, H. Hosono, D.C. Paine, MRS Bulletin 32 (2007) 242.

[5] T. Minami, Semicond. Sci. Technol. 20 (2005) 35.

[6] J.F. Wagner, D.A. Keszler, R.E. Presley, Transparent Electronics, Springer, New York, 2008.

[7] D.S. Ginley, H. Hosono, D.C. Paine, Handbook of Transparent Conductors, Springer, New York, 2010.

[8] A. Bourlange, D.J. Payne, R.G. Egdell, J.S. Foord, P.P. Edwards, M.O. Jones, A. Schertel, P.J. Dobson, J.L. Hutchison, Appl. Phys. Lett. 92 (2008) 092117.

[9] S. Limpijumnong, P. Reunchan, A. Janotti, C.G. Van de Walle, Phys. Rev. B 80 (2009) 193202.

[10] P.D.C. King, R.L. Lichti, Y.G. Celebi, J.M. Gil, R.C. Vilo, H.V. Alberto, J. Piroto Duarte, D.J. Payne, R.G. Egdell, I. McKenzie, C.F. McConville, S.F.J. Cox, T.D. Veal, Phys. Rev. B 80 (2009) 081201(R).

[11] T. Tomita, K. Yamashita, Y. Hayafuji, H. Adachi, Appl. Phys. Lett. 87 (2005) 051911.

[12] S. Lany, A. Zunger, Phys. Rev. Lett. 98 (2007) 045501.

[13] P.D. King, T.D. Veal, J. Phys. Condens. Matter 23 (2011) 334214.

[14] H. Kim, J.S. Horwitz, G.P. Kushto, Z.H. Kafafi, D.B. Chrisey D(2001) Appl. Phys. Lett. 79 (2001) 284.

[15] K. Ellmer, Nat. Photonics 6 (2012) 809.

[16] W. Seiler, M. Nistor, C. Hebert, J. Perrière, Solar Energy Mater. & Solar Cells 116 (2013) 34.

[17] G.B. González, J.B. Cohen, J-H. Hwang, T.O. Mason, J. Appl. Phys. 89 (2001) 2550.

[18] P. Agoston, K. Albe, R.M. Nieminen, M.J. Puska, Phys. Rev. Lett. 103 (2009) 245501.

[19] O. Bierwagen, J.S. Speck, Appl. Phys. Lett. 97 (2010) 072103.

[20] S. Naseem, I.A. Rauf, K. Hussain, N.A. Malik, Thin Solid Films 156 (1988) 161.

[21] J. Stankiewicz, F. Villuendas, R. Alcalá, Appl. Phys. Lett. 96 (2010) 192108.

[22] C. Persson, A. Zunger, Phys. Rev. Lett. 91 (2003) 266401.

[23] J. Stankiewicz, M.P. Lozano, F. Villuendas, Phys. Rev. B 85 (2012) 125306.

[24] O. Bierwagen, J.S. Speck, T. Nagata, T. Chikyow, Y. Yamashita, H. Yoshikawa, K. Kobayashi, Appl. Phys. Lett. 98 (2011) 172101.

[25] G. Frank, H. Köstlin, Appl. Phys. A: Solids Surf. 27 (1982) 197.

[26] E.J. Tarsa, J.H. English, J.S. Speck, Appl. Phys. Lett. 62 (1992) 2332.

[27] N. Tripathi, S. Rath, V. Ganesan, R.J. Choudhary, Appl. Surface Sci. 256 (2010) 7091.

[28] R.K. Gupta, N. Mamidi, K. Ghosh, S.R. Mishra, P.K. Kahol, J. Optoelectron. Adv. M. 9 (2007) 2211.

[29] F. Schmidt, D. Splith, S. Müller, H. von Wenckstern, M. Grundmann, phys. stat. sol. (b) 252 (2015) 2304.

[30] H. Izumi, F.O. Adurodija, T. Kaneyoshi, T. Ishihara, H. Yoshioka, M. Motoyama, J. Appl. Phys. 91 (2002) 1213.

[31] A. Khodorov, M. Piechowiak, M.J.M. Gomes, Thin Solid Films 515 (2007) 7829.

[32] C.R.M. Grovenor, J. Phys. C: Solid State Phys. 18 (1985) 4079.

[33] D.B. Chrisey, G.K. Hubler, Pulsed Laser Deposition of Thin Films, Wiley, New York, 1994.

[34] M. Matsuoka, K. Ono, Appl. Phys. Lett. 53 (1988) 1393.

[35] P.B. Barna, M. Adamik, Science and Technology of Thin Films, World Scientific Publishing, Singapore, 1995.

[36] Z.X. Mei, Y. Wang, X.L. Du, Z.Q. Zeng, M.J. Ying, H. Zheng, J.F. Jia, Q.K. Xue, Z. Zhang, J. Cryst. Growth 289 (2006) 686.

[37] N.F. Mott, Philos. Mag. 19 (1969) 835.

[38] B.I. Shklovskii, A.L. Efros, Electronic Properties of Doped Semiconductors, Springer–Verlag, 1984.

[39] N. Preissler, O. Bierwagen, A.T. Ramu, J.S. Speck, Phys. Rev. B 88 (2013) 085305.

[40] Y-L. Huang, S-P. Chiu, Z-X. Zhu, Z-Q. Li, J-J. Lin, J. Appl. Phys. 107 (2010) 063715.

[41] P. Sheng, Phys. Rev. B 21 (1980) 2180.

[42] J. Ederth, P. Johnsson, G.A. Niklasson, A. Hoel, A. Hultåker, P. Heszler, C.G. Granqvist, Phys. Rev. B 68 (2003) 155410.

[43] D.L. Greenaway, G. Harbeke, Optical Properties and Band Structure of Semiconductors, Pergamon Press, 1968.

[44] R.L. Weiher, R.P. Ley, J. Appl. Phys. 37 (1966) 299.

[45] M. Grundmann, The Physics of Semiconductors, Springer Berlin Heidelberg New York, 2006.